JOURNAL OF GUIDANCE, CONTROL, AND DYNAMICS
Vol. 15, No. 6, November-December 1992

Testing Electrostatically Suspended Gyroscopes Using Trapped Magnetic Flux and Superconducting Sensors

S. Feteih*
Florida State University, Tallahassee, Florida 32316
and
G. M. Keiser,† J. V. Breakwell,‡ and Y. M. Xiao§
Stanford University, Stanford, California 94305

This paper presents the results of dynamical testing of an electrostatically levitated, spherical gyroscope that has a superconducting coating. These results are used to verify and to assess the characteristics and the performance of these gyroscopes in preparation for the Stanford Relativity Experiment (also known as Gravity Probe B) space mission intended for 1996. During this mission the angular drift of the spin axis of a spinning gyroscope will be measured during a period of one full year or more in orbit. This measured drift rate will be compared with the theoretical drift rate as predicted by the general theory of relativity. Research presented here shows that it is possible to measure the time history of the spin vector of a spherical gyroscope with respect to two mutually perpendicular pickup loops in a Helmholtz configuration using the dipole component of the magnetic trapped flux inside the gyroscope. With the use of the time history of the gyroscope spin axis, it is possible to estimate the gyroscope characteristics, in particular its mass unbalance. The measurements recorded during this research are unique in a sense that it is the first time a superconducting sensor in conjunction with trapped magnetic flux was used to determine the orientation of the spin vector of a nearly perfect spherical gyroscope.

Nomenclature

$A, \Delta A$ = amplitude, estimated error in amplitude of FFT routine
a = mass unbalance vector, cm
B_x = SQUID bias along $(\hat{x}_p)$
B_y = SQUID bias along $(\hat{y}_p)$
B_z = SQUID bias along $(\hat{z}_p)$
c = speed of light
DC = traped flux vector parallel to ω
DC_x = DC component along $\hat{x}_p$
DC_y = DC component along $\hat{y}_p$
DC_z = DC component along $\hat{z}_p$
e = charge of electron
g = gravitational acceleration
$I_\oplus$ = Earth's moment of inertia
l = harmonic number
$M_\oplus$ = mass of the Earth
m_e = mass of the electron
m_g = mass of the gyroscope
$\hat{N}$ = unit vector along geographical north
q = quantitization error
r = gyro position vector in orbit
T = trapped flux dipole component
T_f = friction torque
T_{mu} = mass unbalance torque
T_n = trapped flux normal to ω
$\hat{V}$ = unit vector along local vertical
v = gyro velocity vector in orbit
$\hat{x}_{hv}$ = local south
$\hat{y}_{hv}$ = local west
$\hat{z}_{hv}$ = local vertical
$\hat{x}_p$ = axis normal to large pickup loop
$\hat{y}_p$ = axis normal to small pickup loop
$\hat{z}_p$ = axis normal to middle pickup loop
α = ratio of absolute scale factors of small/middle loop
β = ratio of absolute scale factors of large/middle loop
$\Delta\phi_\omega T_p$ = phase angle between T and ω
$\theta_{\omega p}$ = angle between ω and $\hat{z}_p$
ρ_c = niobium coating density
ρ_g = quartz gyroscope density
$\Phi, \Delta\Phi$ = phase angle, estimated error in phase of FFT routine
$\phi_{\omega p}$ = angle between ω and $\hat{x}_p$
ω = gyro spin vector
ω_{eff} = observed precession rate in the lab
ω_p = gyro precession rate
$\omega_\oplus$ = Earth's angular velocity vector

Received Oct. 29, 1990; revision received May 31, 1991; accepted for publication June 3, 1991.

*Assistant Professor, Department of Mechanical Engineering, P.O. Box 2175. Member AIAA.
†Senior Research Associate, Gravity Probe B Program, W. W. Hansen Experimental Physics Laboratory.
‡Professor, Department of Aeronautics and Astronautics. Fellow AIAA.
§Research Associate, Gravity Probe B Program, W. W. Hansen Experimental Physics Laboratory.

I. Introduction

Gravity Probe B Background

GRAVITY Probe B (GP-B) experiment is a program whose objective is to put a nearly perfectly round gyroscope in a purely gravitational polar orbit (by compensating for all external disturbances in orbit) and then to measure the precession of its spin axis with respect to a distinct reference star (an inertial reference frame) during one full year in orbit. This measured angular drift will be compared with the theoretical value based on the general theory of relativity, as calculated by L. I. Schiff[1] in his formula:

$$\Omega = \frac{3GM_\oplus}{2c^2r^3}(r \times v) + \frac{GI_\oplus}{c^2r^3}\left[\frac{3r}{r^2}(\omega_\oplus \cdot r) - \omega_\oplus\right]$$

The precession in a polar orbit, as previously described, consists of two terms: The first (in the orbit plane), known as

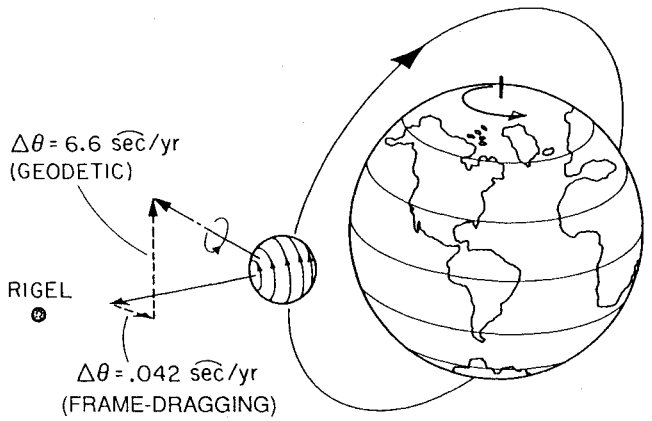

Fig. 1 Geodetic and frame-dragging precession for an Earth-orbiting gyroscope.

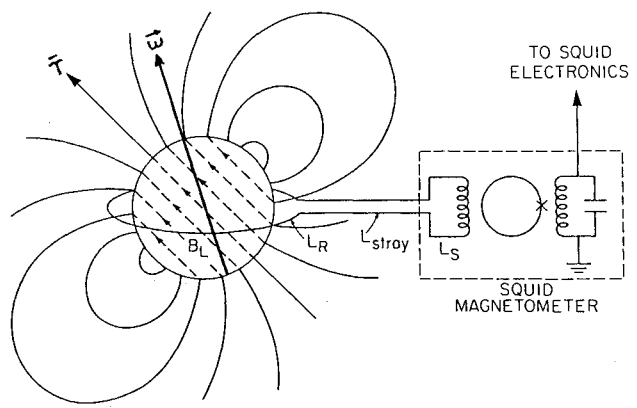

Fig. 2 Concept of trapped flux and readout system.

the geodetic precession, is due to the orbital motion of the spinning gyroscope about the Earth, also known as spin-orbit coupling; the second (normal to the orbit plane), known as frame-dragging, is due to coupling between the spin of the gyroscope and the rotation of the Earth, also known as spin-spin coupling. This latter term is the result of a frame-dragging phenomenon in which a rotating massive body (e.g., the Earth) drags the space-time frame with it. Based on the Schiff formulation,[1] the predicted magnitudes for the geodetic and the frame-dragging precessions of the gyroscope are 1.0181×10^{-12} rad/s (2.1×10^{-7} deg/h) and 6.4965×10^{-15} rad/s (1.34×10^{-9} deg/h), respectively, for a gyroscope in a 650 km polar orbit (see Fig. 1).

The outcome of the GP-B experiment would be to confirm or to refute the general theory of relativity by checking one of its fundamental results: the precession of the spin axis of spinning mass in a purely gravitational orbit.

To measure these precession rates accurately, the drift rate of the gyroscope due to classical (Newtonian) torques should be significantly smaller than the drift rate due to these relativistic effects. The goal of this experiment is to produce a gyroscope where the drift rates due to classical torques are less than 6.3×10^{-17} rad/s (1.3×10^{-11} deg/h). The current requirements on the gyroscopes are that the mass unbalance be less than 50 nm, the rotor asphericity $\Delta r/r$ less than 10^{-6}, and the fractional differences in the moments of inertia $\Delta I^r/I$ less than 10^{-6}. Careful analysis[2,3] of the classical (Newtonian) torques on the gyroscope shows that with an orbit averaged acceleration of less than 10^{-11} g and spinning at 170 Hz, the gyroscope will meet the goals of the experiment.

The objective of this research is to determine the physical characteristics of these gyroscopes by measuring the drift rate of a slowly spinning (1–5 Hz) gyroscope in a 1-g environment. Under these conditions the drift rate is enlarged and the physical characteristics of the gyroscope may be determined from the measured drift rate. These dynamically determined characteristics serve as an additional check on the measurements of rotor density homogeneity, rotor asphericity, and coating thickness variation, which are routinely made during the production of the rotor.

To measure the drift rate of the gyroscope, the magnetic flux, which is trapped in the superconducting coating of the spinning gyroscope was used to determine orientation of the gyroscope spin axis (in a laboratory fixed reference frame) at any given time. This trapped magnetic flux induces currents in superconducting pickup loops that encircle the gyroscope. These currents are, in turn, measured by the SQUID magnetometers.[4] In general, this trapped magnetic flux produces not only a dipole magnetic field but also components of the higher order magnetic multipoles. However, by using two perpendicular pairs of pickup loops, each one in a Helmholtz configuration, it is possible to determine the orientation of the rotor's spin axis to sufficient accuracy using the dipole approximation.

Previous Related Work

To improve the performance of the mechanical gyroscope, the idea of suspending it using an electrostatic or electromagnetic field (to get rid of mechanical friction) was introduced first by A. Nordsieck in 1952, followed by H. W. Knoebel in 1964,[5] both from the University of Illinois. At the time of its introduction, the electrostatic suspended vacuum gyroscope (ESVG) has an estimated uncompensated drift rate of 4.8×10^{-7} rad/s (10^{-1} deg/h) and a potential compensated drift rate of 4.8×10^{-10} rad/s (10^{-4} deg/h). Extensive testing of ESVGs confirmed these initial estimates. The significant improvement in the uncompensated drift rate required by the GP-B experiment is only possible because of the extremely low average acceleration levels that may be achieved in a drag-free satellite.

Extensive work has been done on calculations of the gyroscope drift rate due to the mass unbalance and residual rotor asphericity in the electrostatic field that are used to support the gyroscope. In 1968 G. A. Matchett et al.[6–10] investigated suspension torques resulting from the shape of an axisymmetrical spherical gyroscope in a housing where the hexahedral electrodes almost entirely cover the interior of the housing. They expanded the spin-averaged shape of the gyroscope in a cosine series and calculated the torques due to the first seven terms of this cosine series expansion.

In 1980 and 1982, P. Eby and W. Darbro[11,12] of NASA Marshall Space Flight Center used an approach similar to Matchett's to calculate the electrostatic torques on a gyroscope in the planned GP-B housing where the six electrodes are circular. Using numerical techniques, they evaluated the torques due to rotor asphericities for the first 20 terms in the cosine series expansion of the rotor shape and for the planned orientation of the gyroscope spin axis in the GP-B experiment.

In 1985, G. M. Keiser[13,14] analytically calculated the electrostatic torques for the GP-B gyroscope by expanding the gyroscope shape in terms of spherical harmonics and using rotation matrices to transform from the rotor-fixed frame to the housing-fixed frame. By using these techniques he was able to calculate analytically the electrostatic torques on the gyroscope for an arbitrary gyroscope shape with any orientation for its spin axis. These calculations have been used to determine the requirements on the physical characteristics and acceleration levels of the GP-B gyroscopes.

Conventional ESVGs have relied on an optical pattern or a radial mass unbalance to determine the orientation of the gyroscope's spin axis. Such readout systems are enormously simplified if the polhode motion is damped out[15] so that the gyroscope's spin axis coincides with its maximum inertia axis. Also,

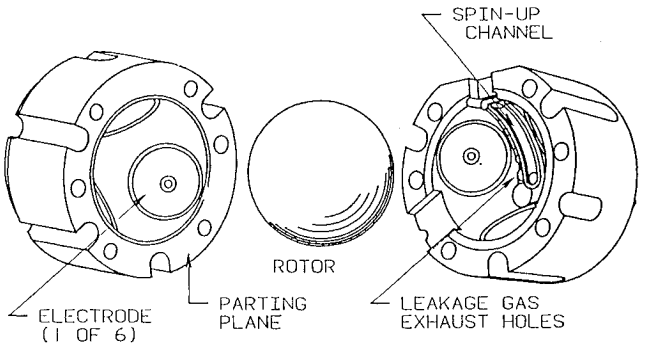

Fig. 3 Gyroscope housing.

operating in this fashion makes the spin-averaged properties of the gyroscope, such as mass unbalance and asphericity, independent of time and thereby simplifies the mathematical process of compensation for the gyroscope drift rate. However, to ensure that the rotor spin axis does not deviate from the principal axis, it is necessary to have a fractional difference in the moment of inertia (10^{-4} to 10^{-1}). For the GP-B gyroscopes such a large difference in the moments of inertia would lead to an unacceptably large drift rate, because of the interaction of the gradient in the gravitational field with the mass quadrupole moment of the rotor (which is proportional to the fractional difference in the moments of inertia).

Additional requirements on the GP-B gyroscope readout are that it be sufficiently accurate (it must be capable of resolving 1 marc-s/yr in a small fraction of a year) and that it be insensitive to small displacements of the gyroscope from its centered position. These considerations led to a unique gyroscope readout based on the London moment of a spinning superconductor (shown in Fig. 2). A spinning superconductor develops a magnetic dipole field along its spin axis.[18] Since the direction of the dipole field is independent of the orientation of the spin axis within the body of the gyroscope, it is no longer necessary to damp out the polhode motion to have an accurate readout. Laboratory work has demonstrated that such readout, when used with a dc SQUID magnetometer, will have sufficient accuracy to resolve changes of less than 1 marc-s/yr in several days or less.[16,18]

Development of these gyroscopes and the readout methods has been underway at Stanford University for a number of years. A precise London moment readout was first used with a superconducting gyroscope in 1978.[3] This readout is expected to work well for the GP-B flight experiment, but it is not ideal for laboratory testing, which is the subject of this paper. The requirements on the SQUID dc stability for a nongimballed housing are very stringent, and the residual magnetic field at the location of the gyroscope must be less than 1μ Gauss. In addition, since the London moment signal is proportional to the spin speed, the sensitivity is greatly reduced for any testing that is done at low spin speeds. For the purpose of modeling the gyroscope torques, the London moment readout has an obvious weakness: It is insensitive to the motion of the spin axis within the body. With these considerations in mind, work has been underway at Stanford for a number of years to use the trapped magnetic flux in the superconducting gyroscope as an additional means of reading out the orientation of the gyroscope with respect to mutually perpendicular readout coils.

In 1982 G. M. Keiser and B. Cabrera[19] used the SQUID along with the trapped magnetic flux to determine the orientation of the spin axis of a gyroscope with $\Delta I/I = 10\%$. By assuming that the motion of the spin axis within the body followed the polhode path for a torque-free symmetric gyroscope, they were able to determine the orientation of the spin axis with respect to the pickup loop and the orientation of the spin axis within the body.

For gyroscopes with smaller $\Delta I/I$ the situation is more complicated. If the distribution of trapped flux within the rotor at any given time is known, then it is possible to determine the orientation of the spin axis. Conversely, if the time history of the rotor spin axis is known, then it is possible to determine the distribution of the trapped flux. One purpose of this paper is to demonstrate that by carefully designing the configuration of the pickup loops, the dipole approximation for the trapped flux distribution produces a gyroscope readout of sufficient accuracy.

The notion of using superconducting sensors to measure the orientation of the spin vector of an unmarked nearly perfect spherical gyroscope is rather new and was never used before. This is considered to be the main contribution of this research.

Gyroscope Test Facility

To meet operational requirements the gyroscope was mounted in an apparatus with a controlled environment known as Gyroscope Test Facility (GTF).[23] The measurements reported here were made in GTF in the following environment:

1) temperature: $5°K - 300°K$
2) pressure: ($10^{-3} - 10^{-10}$ Torr)
3) magnetic field: 10^{-3} G

Typically, measurements reported here were made at 5°K with the pressure at the gyroscope in the range of $10^{-5} - 10^{-6}$ Torr. In addition, this facility provided high voltage cables that were used to connect the electrostatic suspension system (which operated at room temperature) to the gyroscope. The other major subsystem in this facility was the vacuum system and the plumbing required to provide the helium spinup gas to the gyroscope.

Gyroscope Readout

In the laboratory the magnetic readout of the gyroscope used two or three pairs of orthogonal pickup loops in a Helmholtz configuration connected to rf SQUIDs. The axis joining the centers of each pair of coils (which constitute one loop) passes through the center of the gyroscope, and each coil of a pair is equidistant from the center of the gyroscope. The centers of the small, medium, and large coils are 1.58, 1.91, and 2.5 cm from the center of the gyroscope, respectively.

The Helmholtz configuration of the pickup loops provides more sensitivity for the dipole component of the trapped flux and no sensitivity for its quadrupole, octapole, or hexadecapole components. Although the pickup loops are sensitive to the higher multipole components of the trapped magnetic field, the magnitude of these components decreases inversely at least as fast as the seventh power of the distance of the loop from the gyroscope. In addition, if the gyroscope is cooled in a uniform magnetic field, the trapped magnetic field has

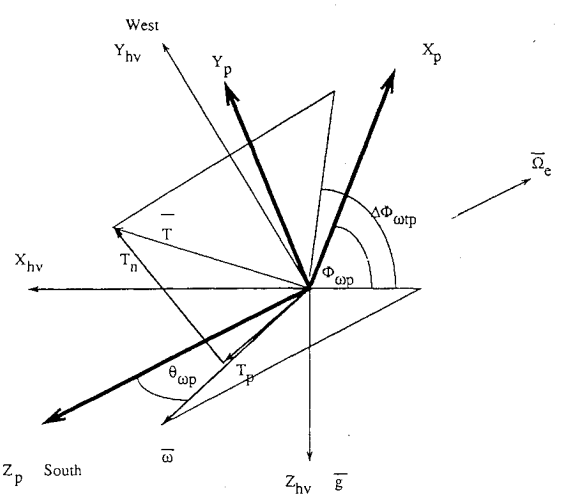

Fig. 4 Reference frames $\{\hat{x}_p, \hat{y}_p, \hat{z}_p\}$ and $\{\hat{x}_{hv}, \hat{y}_{hv}, \hat{z}_{hv}\}$.

mainly a dipole component. Therefore, only the nonuniformities in the residual magnetic field will produce nondipole components of the trapped magnetic flux. For these two reasons, the dipole approximation of the trapped magnetic flux is a good approximation.

Each of the loops in a Helmholtz pair is connected in series and connected through a superconducting transformer to the input of a commercial SQUID magnetometer. The output of the electronic system that enters the SQUID magnetometer is directly proportional to the current flowing to the input terminals of the SQUID, but with an unknown dc offset. This current is proportional to the component of the flux through the pickup loop, which in turn is proportional to the component of the magnetic dipole component normal to the pickup loop T_n.

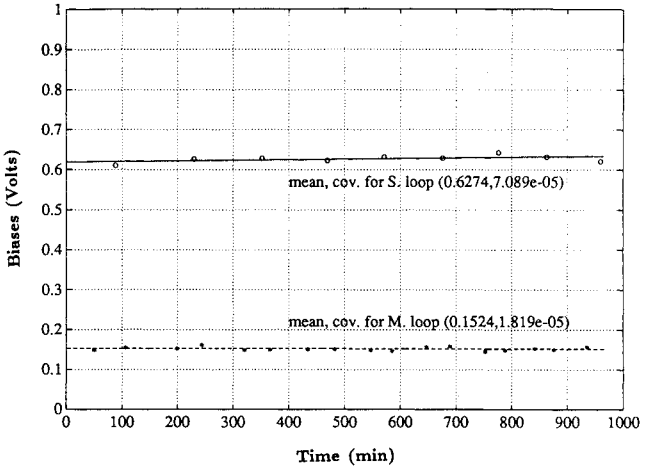

Fig. 5 Biases in the SQUIDs for gyroscope 86-4.

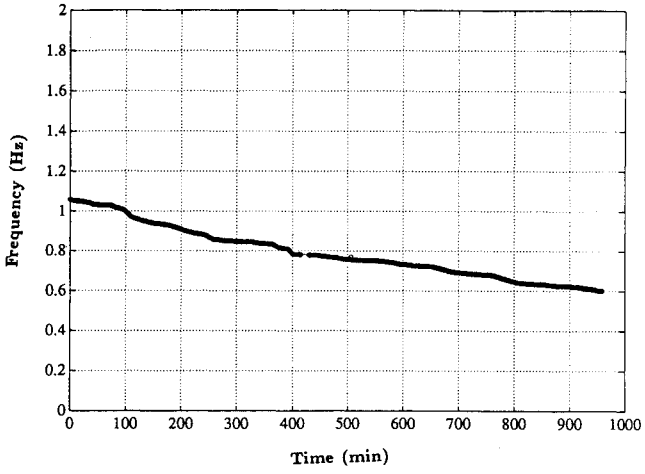

Fig. 6 Time history of the spin speed for gyroscope 86-4.

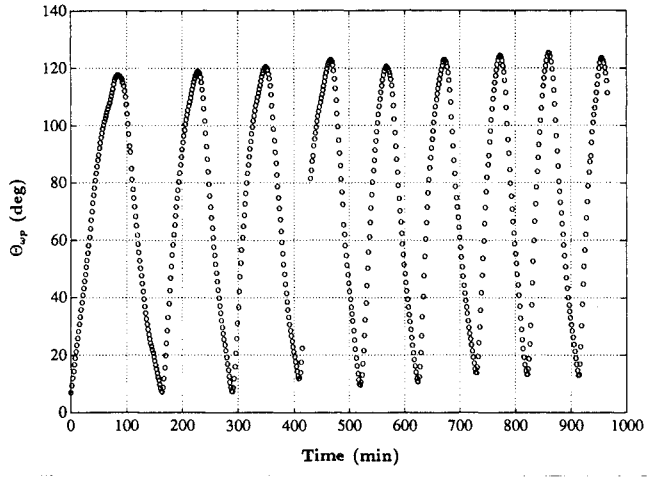

Fig. 7 Time history of the angle $\theta_{\omega p}$ for gyroscope 86-4.

Data from all pickup loops were sampled at a sampling rate of 40 Hz, a 12 bit A/D converter was used. Each 1024 points of data was processed using a fast Fourier transform (FFT) to produce an amplitude and an associated phase at the rotor spin speed and harmonics of the spin speed. The same process is repeated each 90 s for all three loops. This implies that we are sampling at two different frequencies: the first is fast (40 Hz) to determine orientation of spin vector in the lab at a given instant; the second is slower (0.0111 Hz) to keep track of spin axis motion in the laboratory.[23]

Gravity Probe B Gyroscope

The GP-B gyroscope is a spherical ball 1.9 cm in radius (shown in Fig. 3) and made from optically selected fused quartz homogeneous in density to 1 part in 10^6 (Ref. 3). Quartz blocks are ground, lapped, and polished to a spherical shape with a typical asphericity of 25 nm. The sphere is coated with a 2500-nm-thick coating of niobium that is uniform to within 25 nm (bulk niobium is superconducting below 9°K). The niobium coating is deposited using a sputtering technique, which provides good adhesion and acceptable superconducting properties. To measure the coating thickness of the gyroscope, 26 points on the surface of the coating are exposed to a radioactive source and then the backscattered electrons are counted.[20,21] The coating serves as: 1) an equipotential surface for the electric suspension of the gyroscope, 2) a superconductor to generate the London magnetic moment of the spinning gyroscope, and 3) a superconductor to trap the ambient magnetic field within the gyroscope.

Also shown in Fig. 2 is the gyroscope housing that is also made from fused quartz. Three pairs of circular electrodes are used to sense and to control the gyroscope position using 1-MHz and 2-KHz voltages, respectively. The gap between the electrodes and the rotor when the rotor is centered is 31 μm. With this gap the typical potential difference between the electrode and the gyroscope, which is required to levitate the gyroscope, is 700 V rms. Also shown in the same figure is the spinup channel, which is used to spin up the gyroscope to its operating speed by sending a helium gas jet through this channel.

II. Trapped Flux Readout Determination of the Spin Axis

Assumptions

To make use of the trapped flux signature to determine the orientation of the spin vector in the $\hat{x}_p, \hat{y}_p, \hat{z}_p$ reference frame, we assumed the following:

1) The trapped magnetic field is a dipole, in other words we neglected the presence of higher harmonics of trapped flux. This was later confirmed by the ratio of higher harmonics to the 1st harmonic in the output of the FFT data reduction program (less than 3%).

2) The magnetic trapped flux is fixed inside the gyroscope during one data acquisition period (22 s).

3) The median position of the spin vector ω is fixed in the laboratory during one data acquisition period (22 s).

4) A kinematical model to extract spin vector orientation in the laboratory was used.

5) No additional sources of magnetic fields, such as eddy currents in normal metals, were significant.

Scale Factor Determination

Conversion from magnetic flux (in Gauss-cm^2) sensed by the pickup loops into voltages indicated by the SQUIDs was achieved using an absolute scale factor associated with each pickup loop. These three absolute scale factors associated with

Table 1 Determining the correct quadrant of $\phi_{\omega p}$ given $\theta_{\omega p}$, μ_3, and μ_4

$\theta_{\omega p} \in \{0, \pi/2\}$	
$\mu_3 < 0$ and $\mu_4 > 0$	$\phi_{\omega p} \in \{0, \pi/2\}$
$\mu_3 < 0$ and $\mu_4 < 0$	$\phi_{\omega p} \in \{\pi/2, \pi\}$
$\mu_3 > 0$ and $\mu_4 > 0$	$\phi_{\omega p} \in \{3\pi/2, 2\pi\}$
$\mu_3 > 0$ and $\mu_4 < 0$	$\phi_{\omega p} \in \{\pi, 3\pi/2\}$
$\theta_{\omega p} \in \{\pi/2, \pi\}$	
$\mu_3 < 0$ and $\mu_4 > 0$	$\phi_{\omega p} \in \{3\pi/2, 2\pi\}$
$\mu_3 < 0$ and $\mu_4 < 0$	$\phi_{\omega p} \in \{\pi, 3\pi/2\}$
$\mu_3 > 0$ and $\mu_4 > 0$	$\phi_{\omega p} \in \{0, \pi/2\}$
$\mu_3 > 0$ and $\mu_4 < 0$	$\phi_{\omega p} \in \{\pi/2, \pi\}$

Table 2 Spin-down and precession torques (dyne-cm) due to friction and mass unbalance for gyroscope 86-4

	T_f	T_{mu}
worst case	0.058	0.159
best case	0.00117	0.159
nominal case	0.0062	0.159

Table 3 Measured SQUIDs biases, and standard deviation (σ)

Gyroscope	Gyroscope 86-4		
Pickup loop	Small	Medium	Large
Bias (V)	0.6275	0.1524	n/a
σ	7.1×10^{-5}	1.82×10^{-5}	n/a

small, medium, and large pickup loops were reduced to two relative scale factors: α and β. The first is the ratio of the absolute scale factor for the small pickup loop to the absolute scale factor of the middle pickup loop, while the second is the ratio of the absolute scale factor for the large pickup loop to the absolute scale factor for the middle one.

Calibration of each SQUID and its pickup loop was achieved through the following steps:

1) Calculating the mutual inductance between the pickup loop and a calibration coil.

2) Measuring the response of the SQUID to a known current injected in the calibration coil.

3) Calculating the flux through the pickup loop for a given magnetic dipole moment of the trapped magnetic field.

The limiting factor in this calibration process is the accuracy with which the mutual inductance between the calibration coil and the pickup loop may be calculated (based on the dimensions of the two loops). Accuracy with which this mutual inductance has been calculated is estimated to be 5%. The induced signal in the pickup loop is filtered using a low pass filter (in the form of a damping cylinder); then it is amplified and converted into voltage difference using the SQUID electronics.

The relative scale factor of the small to the middle pickup loops used during testing of gyroscope 86-4 was determined using such technique and was found to have a value of 2.2.

Reference Frames

Two reference frames were used for this analysis: the first one attached to the pickup loops $\{\hat{x}_p, \hat{y}_p, \hat{z}_p\}$, the second one to local horizontal and vertical planes $\{\hat{x}_{hv}, \hat{y}_{hv}, \hat{z}_{hv}\}$ as shown in Fig. 4.

Data Analysis

To deduce the time history of the orientation of the gyroscope spin axis in $\{\hat{x}_p, \hat{y}_p, \hat{z}_p\}$ reference frame, we used the time history of the amplitudes and phases associated with the middle and small pickup loops (as described in Refs. 21 and 23).

Equations (A16-A19) in the Appendix give analytical expression for the four parameters $\phi_{\omega p}$, $\theta_{\omega p}$, T_n, and $\Delta\phi_{\omega Tp0}$.

Equation (A16) indicates that there is an ambiguity in determining the exact quadrant {1st or 2nd} where the angle $\theta_{\omega p}$ lies. This ambiguity could be solved at the start of each run, based on our knowledge of the initial quadrant of the spin vector in the laboratory, and during the rest of the run by forcing the $\theta_{\omega p}$ to continue into the second quadrant when it approaches $\pi/2$ from below, and by forcing it to continue into the first quadrant when it approaches $\pi/2$ from above. This was possible only because the trace of ω in the lab was smooth enough and continuous (due to minimal perturbations from the motion of ω inside the gyroscope) to the point that we could predict its orientation when it was close to the separation line between the 1st and the 2nd quadrant. Once the ambiguity in the angle $\theta_{\omega p}$ was resolved, the angle $\phi_{\omega p}$ was determined in full using the signs of μ_3 and μ_4 as given in Eqs. (A14) and (A15) in the Appendix. The results are summarized in Table 1.

Estimating Biases in the SQUIDs

The output of the data reduction routine consisted of two main parts: the first is the trapped flux component normal to ω (trapped flux at the spin frequency); the second is the trapped flux component parallel to ω together with unknown SQUID biases (dc component). We made use of both compo-

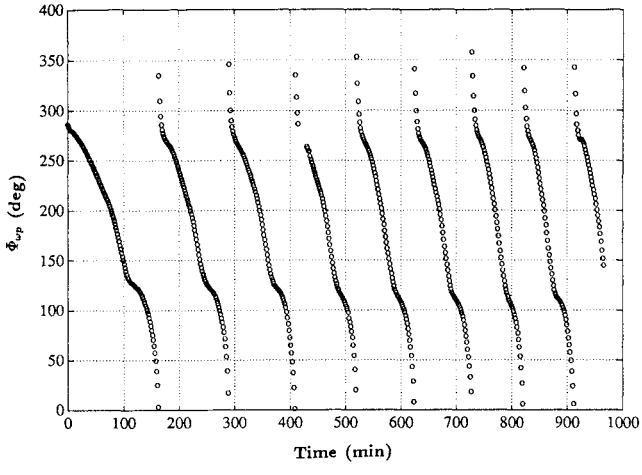

Fig. 8 Time history of the angle $\phi_{\omega p}$ for gyroscope 86-4.

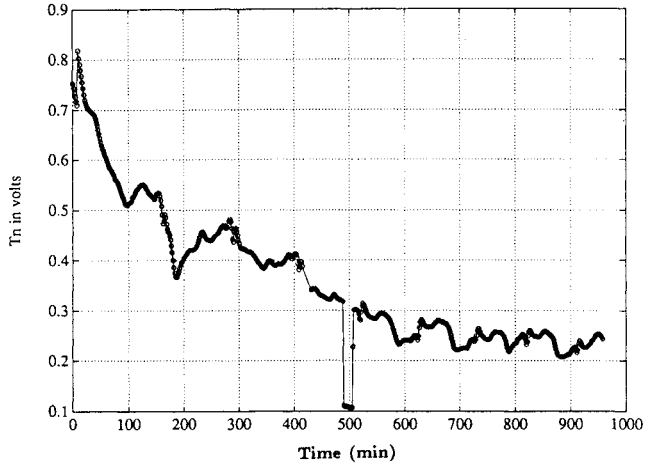

Fig. 9 Time history of trapped flux component normal to ω for gyroscope 86-4.

nents in order to estimate the biases associated with different loops.

An expression relating the dc measurement of each loop $\{DC_x, DC_y, \text{and } DC_z\}$ to the bias associated with the same loop $\{B_x, B_y, \text{and } B_z\}$ can be written as follows:

$$DC_z = B_z + DC\cos(\theta_{\omega p}) \quad (1)$$

$$DC_y = B_y + DC\sin(\theta_{\omega p})\sin(\phi_{\omega p}) \quad (2)$$

$$DC_x = B_x + DC\sin(\theta_{\omega p})\cos(\phi_{\omega p}) \quad (3)$$

The trapped flux-dependent term in Eq. (1) vanishes when $\theta_{\omega p} = \pi/2$. This can be picked directly from the time history of the angle $\theta_{\omega p}$ (shown in Fig. 7). At this point the output of the SQUID is equal to the bias, which identifies the bias associated with the medium loop. In a similar way the trapped flux dependent term in Eq. (2) vanishes when $\phi_{\omega p} = \pi$. At this point the output of the SQUID is equal to the bias, which identifies the bias associated with the small loop.

Biases associated with small and medium pickup loops used for testing gyroscope 86-4 were calculated using the algorithm presented earlier and are shown in Fig. 5.

Sources of Errors

Several assumptions were made in order to make use of the trapped flux signal to measure the time history of the spin vector in the laboratory, these assumptions were listed in Sec. II. As a result of these assumptions and as a result of operational constraints, several sources of errors were identified and are listed below.

Higher Harmonics Error

This error results from neglecting the presence of higher harmonics of the trapped flux, this error appears in the measured amplitude associated with each pickup loop. The higher harmonics error was estimated to be typically 3% (based on the ratio of higher to first harmonic in the FFT output program).

Amplitude and Phase Error

This is an error in estimating the amplitudes and phases associated with each pickup loop using the FFT data reduction routine. It results from the fact that an FFT is a discrete process and an amplitude of a sine wave must be determined by interpolating between nearby bins. An estimate of the error in this interpolation routine was made and found to be $\Delta A/A = 0.001$, and $\Delta\Phi = 0.001$ rad for the measured amplitude A and phase ϕ, respectively.

Scale Factor Error

These errors due to uncertainty in relative scale factors calculated based on calibration technique or using spin vector time history in the laboratory.

Quantization Error

These errors are due to quantization effects resulting from the use of a 12-bit A/D converter. These errors q were estimated to be less than $2^{-12} = 2.44 \times 10^{-4}$.

Stationary Error

This error is due to our assumption of a stationary spin vector in the laboratory during one data acquisition period (22 s). It was estimated to be less than 0.05% based on the comparing precession period of 3 h to data acquisition period.

The positions of the spin vector of the gyroscope are measured in the laboratory with respect to the pickup loops but still are absolute position measurements in a sense that each measurement is independent of the one before it and does not affect the following measurements.

III. Determination of the Mass Unbalance

The performance of the spinning gyroscope was assessed using the time history of its spin vector as seen in the laboratory; its history was affected by the Earth's rotation and by the externally applied torques. In the case of an electrostatically supported gyroscope, these torques result from mass unbalance as well as other suspension torques due to asphericity of the gyroscope shape. The mass unbalance of the gyroscope is larger than the coefficients of higher harmonics in shape of the gyroscope because the mass unbalance is a function of the density ratio of the niobium coating to the quartz gyroscope $\rho_c/\rho_g \cong 3$, while the higher harmonics in shape are a function of the asphericity in shape that can be measured by the ratio of the coating's maximum peak-to-valley measurement to the gyroscope's nominal radius (which was calculated based on coating thickness measurements and found to be 3.9×10^{-6} for gyroscope 86-4). In laboratory tests, the drift of the gyro-

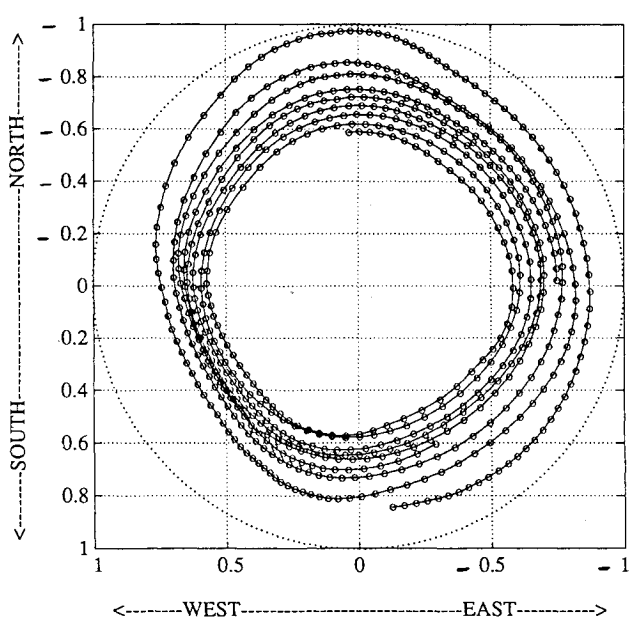

Fig. 10 Projection of ω on local horizontal plane for gyroscope 86-4.

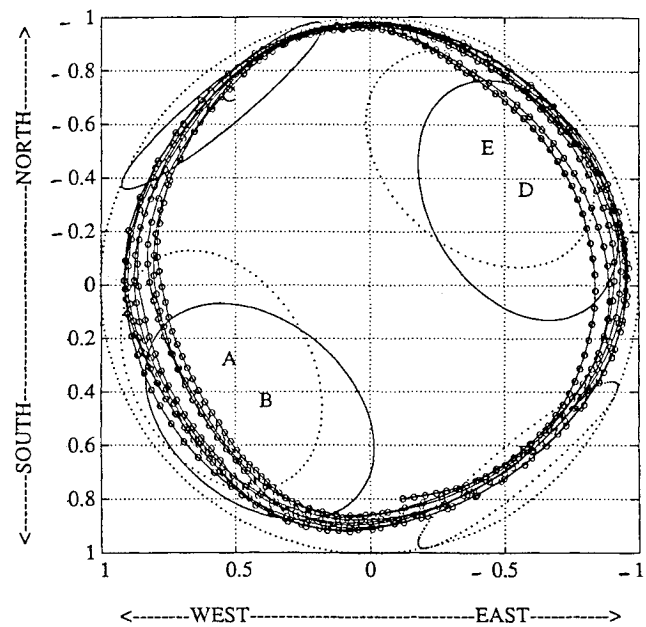

Fig. 11 Projection of a unit vector along ω on local horizontal plane for gyroscope 86-4.

scope spin axis due to relativistic effects was negligible compared to drifts due to Newtonian forces; therefore, it was ignored. In the following section we will estimate the mass unbalance of the spinning gyroscope using the time history of its spin axis in the laboratory.

Assumptions

To determine the mass unbalance and asphericity of the gyroscope from the motion of ω in the laboratory, we made use of the following assumptions:

1) The gyroscope was assumed to be a rigid body, no elasticity effects were considered.

2) The precession torque due to differential drag on the gyroscope was negligible compared to the one due to mass unbalance.

3) No energy exchange takes place between the pickup loop and the gyroscope, i.e., there are no magnetic torques exerted on the gyroscope.

4) The average drift rate of the gyroscope could be determined from the difference in two position measurements.

5) Torques due to asphericity were considered to be small compared with those due to the mass unbalance.

External torques applied to the gyroscope include contributions from mass unbalance, residual gas pressure, asphericity of the gyroscope, and frictional forces. These torques can be classified into two categories: 1) torques resulting in spin-down of the gyroscope (principally due to frictional and drag forces), 2) torques resulting in precession of its spin axis (due to mass unbalance and asphericity).

Spin-Down Torques

To estimate the torques resulting from friction forces on a spherical gyroscope with inertia I and a measured spin-down rate, $d\omega/dt$, the following formula can be used:

$$T_f = I(d\omega/dt) \tag{4}$$

For the case of gyroscope 86-4, the spin-down rate (as shown in Fig. 6) varied from its worst case of 0.36 rad/h to its best case of 7.2×10^{-3} rad/h, with a nominal value of 0.038 rad/h. The worst case refers to the fastest spin-down rate, while the best case is the slowest spin-down rate. The measured frictional forces were the main factor in the gyroscope spin-down rate shown in Table 2, and a comparison between columns 1 and 2 in the same table validates our assumption number 2 mentioned previously.

Precession Torques

Precession torques are torques whose axes are not aligned with the angular momentum of the gyroscope and result in a change in the orientation of the spin axis in an inertially fixed reference frame known as precession. These torques can be attributed to many sources such as mass unbalance, electrostatic suspension forces, magnetic forces, and relativistic torques. The last two were calculated[3] and found to be negligible in comparison with the first two for our study, i.e., ground-based testing of GP-B gyroscopes. We attributed precession torques to two sources:

1) Mass unbalance, which can be written as:

$$\boldsymbol{T}_{\mathrm{mu}} = \boldsymbol{a} \times m_g \boldsymbol{g} \tag{5}$$

2) Asphericity of the gyroscope. These torques are investigated in Refs. 22 and 23 and are referred to as electrostatic suspension torques due to asphericity.

Torques due to asphericity are smaller than torques due to mass unbalance, as discussed in Ref. 23.

Results for Gyroscope 86-4

Gyroscope 86-4 was tested for 16 hours continuously; Fig. 6 shows the time history of ω with an initial spin frequency of 1.2 Hz and a spin-down rate of 0.038 rad/h. The angles $\theta_{\omega p}$, and $\phi_{\omega p}$, which describe the orientation of the spin vector in the laboratory in $\{\hat{x}_p, \hat{y}_p, \hat{z}_p\}$ reference frame are shown in Figs. 7 and 8. They are determined using the model presented in the Appendix and explained in Sec. II. The periodicity in both angles reflects the precession of the spin vector in the laboratory.

Figure 9 shows the time history of the trapped flux component normal to the spin vector inside the gyroscope.

Trapped flux component parallel to ω inside the gyroscope is detected by pickup loops as a dc component. These dc components along the $\hat{y}_p$ and $\hat{z}_p$ axes were recorded by the small and medium loops whose normals are aligned with the $\hat{y}_p$ and $\hat{z}_p$, respectively.

The projection of ω on the local horizontal plane is shown in Fig. 10. The spin-down rate (0.038 rad/h) is reflected in the spiraling inward of the trace of ω; it also shows that the spin

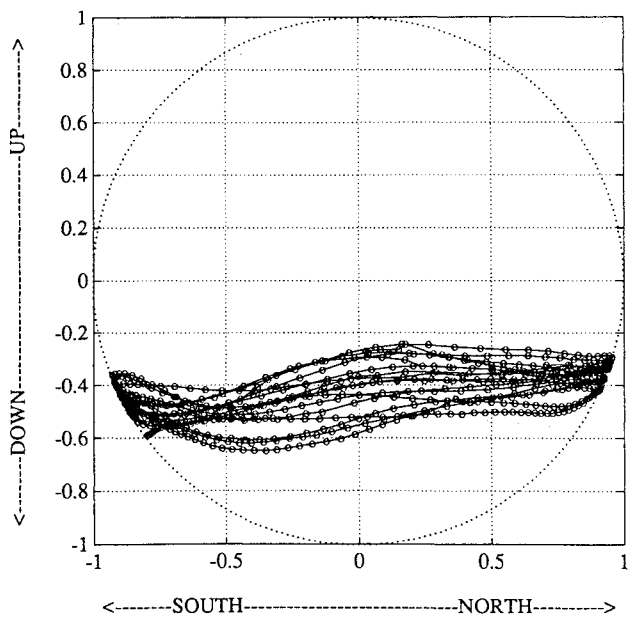

Fig. 12 Projection of ω on local vertical plane for gyroscope 86-4.

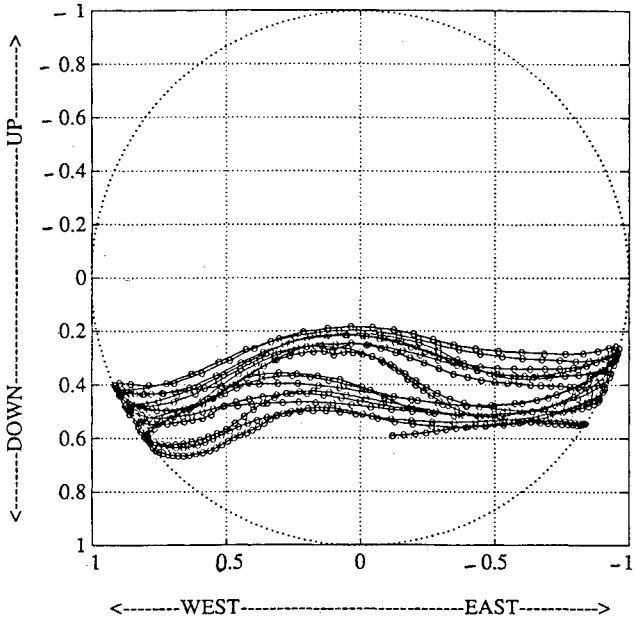

Fig. 13 Projection of ω on local vertical plane for gyroscope 86-4.

vector follows an eastward precession, and its initial orientation points to the geographical south.

Figure 11 shows the projection on the local horizontal plane of a unit vector along the spin axis. The nearly circular path indicates that the main driving torque is due to a local vertical force (gravity acceleration applied to the component of the mass unbalance parallel to ω).

The repeatability of the trace of the unit vector on a local horizontal plane (in other words, the deviation from a nearly perfect circle) is shown in Fig. 11. After correlating these locations of discrepancies from a perfect circle to the locations of supporting electrodes, it was clear that the biggest discrepancy took place when ω is closer to the electrodes (A-B, and D-E). These two pairs of electrodes, whose centers are present in the local vertical plane, support the gyroscope against the gravitational acceleration; consequently, they carry the highest voltage differences.

Electrostatic suspension torques resulting from the voltage difference and the asphericity of the gyroscope cause ω to deviate from a perfectly circular pattern. The deviation caused by the electrodes is more apparent in the projection of ω on a local vertical plane (as shown in Figs. 12 and 13).

The time rate of change of the spin vector in the laboratory can be written as

$$\omega = \omega_{eff} \times \omega \tag{6}$$

where precession in the laboratory can be divided into two components: the first due to the Earth's spin rate; while the second is due to Newtonian precession due to mass unbalance and suspension torques, and can be written as

$$\omega_{eff} = -\omega_{\oplus} \hat{N} + \omega_p \hat{V} \tag{7}$$

For the case of gyroscope 86-4, the inertia difference $\Delta I/I$ was very small; as a result, the mass unbalance component parallel to ω inside the gyroscope is nearly constant due to the fact that the motion of the spin vector inside the gyroscope with respect to a body fixed reference frame was very small.

From Fig. 10 we see that the spin vector took 3.4 h to complete one full precession cycle. This implies that

$$\omega_{eff} = 6.9\omega_{\oplus} = 103°/\text{h} \tag{8}$$

and after subtracting the Earth's rotation rate, the gyroscope precession rate can be found to be

$$\omega_p = 1.713 \text{ rad/h} = 97.6°/\text{h} \tag{9}$$

since

$$\omega_p = \frac{m_g m_{up} g}{I\omega} \tag{10}$$

where the mass unbalance parallel component (m_{up}) is defined as

$$m_{up} = \bar{a} \cdot \hat{\omega}$$

and this leads to an m_{up} of 0.0533 μm (2.1 μin) for rotor 86-4, which compares very well with the mass unbalance estimated using coating thickness measurements 0.061 μm.[21,23]

The precession rate of gyroscope 86-4 when translated into orbit condition indicates that it is qualified for the Science Mission, i.e., the lab-estimated mass unbalance (0.0533 μm) in orbit condition will result in precession of the spin axis of the gyroscope less than 1×10^{-12} deg/h (4.848×10^{-18} rad/s or 1 marc-s/yr). This low drift rate is due to the drag-free orbit, which will result in a residual acceleration of $1 \times 10^{-11} g$ instead of the laboratory level of 1 g, and the higher spin frequency of 170 Hz instead of the 1 Hz spin frequency used during laboratory testing.

Stability of Trapped Flux

The trapped magnetic flux is usually assumed to be frozen inside the gyroscope, i.e., its orientation and amplitude do not change with time (with the exception of occasional arcing). This picture was not quite true during testing of the GP-B spinning spherical gyroscopes with 100 μin (2.54 μm) niobium coating. For gyroscope 86-4, Fig. 9 shows that the average value of the normal component of the trapped flux has changed from 0.8 V (1.55×10^{-3} G) to a steady-state value of 0.25 V (4.9×10^{-4} G) in about 10 h.

A number of checks were made to ensure that this observed apparent change in the trapped flux was not due to instrumental errors. The source of this apparent change in the amplitude of the trapped flux is under investigation. It is important to report that this change in the amplitude does not affect the result of this paper since the amplitude of the trapped flux has been factored out in the mathematical model as shown in the Appendix.

IV. Discussion and Conclusions

Discussion

Research presented in this paper was inspired by the peculiar features associated with GP-B gyroscopes and by the need to test and to assess their characteristics as well as their performance in preparation for the Science Mission. To achieve the Science Mission objectives, GP-B gyroscopes differ from the conventional ones in having a very small difference in moments of inertia to minimize the gravity gradient torques exerted on the gyroscopes in orbit.

The readout system represents a major difference between conventional ESVG and GP-B gyroscopes. Conventional ESVG gyroscopes rely on optical patterns and optical sensors in order to determine the orientation of the spin axis inside the housing. For GP-B gyroscopes, SQUIDs in conjunction with trapped magnetic flux (or London moment) were used to determine the orientation of the spin axis inside the housing, this was dictated by the experiment requirement to have a nearly perfect spherical gyroscope. Damping the polhode motion of the gyroscope is another difference between conventional ESVG and GP-B gyroscopes.

Coating thickness measurements, though limited in number to only 26 independent measurements, were used to estimate the mass unbalance and inertia ratio for gyroscope 86-4.[21,23] The estimated mass unbalance (using coating thickness measurements) of 61 nm for gyroscope 86-4 agrees well with the value of 53 nm measured for the component of the mass unbalance parallel to the spin axis (using precession information as shown in Sec. III and Ref. 23).

The calculated inertia ratio (using coating thickness measurements[21]) of 5.7×10^{-6} for gyroscope 86-4 could not be confirmed experimentally using dynamical testing but was greatly reflected in the smooth trace of the spin vector in the laboratory. That implies very little variation in the relative orientation of the mass unbalance vector with respect to the spin vector.

To determine the orientation of the spin vector ω in the laboratory, we assumed the magnetic trapped flux to be a vector; we further assumed this magnetic trapped flux to be stationary inside the gyroscope during one data acquisition period of 22 s.

Using the time history of the spin vector in the laboratory (based on the ac component of the trapped flux signal) together with the measured component of the trapped flux dipole vector parallel to the spin vector inside the gyroscope (known as dc components), we calculated the biases in the SQUIDs. The numbers obtained show the remarkable stability of the measuring device we used (the SQUID). Long-term stability of the SQUID is well known and was expected; nevertheless, extracting the biases using gyroscope spin axis time history was an indication of the validity of our model and the measured performance of the gyroscope represented by the time history of its spin axis.

The dominant effects on the precession of the spin vector of each gyroscope in a laboratory fixed reference frame were found to be the Earth spin rate and the mass unbalance.

Projection of the spin vector on local vertical planes (discussed in Sec. III and presented in Figs. 12 and 13) shows the effect of electrostatic suspension torques on the spin axis of the gyroscope and its motion in a laboratory fixed reference frame. The trace of the spin vector on the local vertical plane would follow a straight line if the gyroscope was influenced only by its mass unbalance (a local vertical force), but our measurements show that it deviates from that straight line each time it crosses one of the supporting electrodes. This deviation was the result of the asphericity in the shape of the gyroscope and its interaction with the electrostatic suspension system.

One important conclusion of testing gyroscope 86-4 is that the gyroscope is within Science Mission requirements (in terms of precession due to Newtonian forces). The mass unbalance calculated based on coating thickness measurements and precession data would result in a precession less than 1×10^{-12} deg/h or 1 marc-s/yr in the orbit condition (where residual acceleration of $1\times10^{-11}g$ rather than $1g$ and spin frequency of 170 Hz instead of 1 Hz are present).

Dynamical testing of gyroscope 86-4 did not only measure its characteristics and performance but also validated the notion of using the signal of the trapped magnetic flux when recorded using two operational pickup loops in order to measure the time history of the spin vector of an electrostatically levitated unmarked spherical gyroscope in the lab and check for the integrity of the Gyroscope Test Facility.

The use of a superconductor (a SQUID in our study) as a readout system to sense the orientation of a spinning gyroscope (an ESVG in our study) can be expanded to include other types of mechanical gyroscopes. This concept can be useful for future applications for inertial navigation devices and is supported with the current research and development in the area of high temperature superconductivity.

Conclusions

The following conclusions are based on the study conducted and presented in this paper.

1) Measuring the time history of the gyroscope spin axis in the lab was possible using two pickup loops and a dipole model of the trapped magnetic flux.

2) Mass unbalance based on lab precession data (for gyroscope 86-4) indicates that an equivalent mass unbalance will result in a 1 marc-s/yr drift rate in orbit conditions.

3) Mass unbalance is the main contributor to precession of the spin vector in the laboratory, and its size using niobium coating thickness measurements and precession information is consistent.

4) Trapped flux exhibits a decay in amplitude in the first few hours after cooling the gyroscope and spinning it.

Appendix: Two-Loop Analysis

Only two pickup loops were operational when gyroscope 86-4 was tested. The output of the data acquisition system consisted of four measurements: an amplitude and a phase difference associated with each of the two pickup loops. In this Appendix we present the mathematical model we used to calculate the four parameters $\theta_{\omega p}$, $\phi_{\omega p}$, T_n, and $\Delta\phi_{\omega Tp}$ (as defined in Fig. 4) using the output of the small and middle pickup loops. The normal component of the trapped flux can be decomposed into three components along $\hat{x}_p, \hat{y}_p, \hat{z}_p$ axes:

$$T_n x = T_n(\cos\phi_{\omega p}\cos\theta_{\omega p}\cos\Delta\phi_{\omega Tp} + \sin\phi_{\omega p}\sin\Delta\phi_{\omega Tp}) \tag{A1}$$

$$T_n y = T_n(\sin\phi_{\omega p}\cos\theta_{\omega p}\cos\Delta\phi_{\omega Tp} + \cos\phi_{\omega p}\sin\Delta\phi_{\omega Tp}) \tag{A2}$$

$$T_n z = T_n(-\sin\theta_{\omega p}\cos\Delta\phi_{\omega Tp}) \tag{A3}$$

The phase angle between the trapped flux vector $\boldsymbol{T}$ and the spin vector ω projected on the $\hat{x}_p, \hat{y}_p$ plane (and defined as $\Delta\phi_{\omega Tp}$) can be expressed in terms of its initial value and its time rate of change:

$$\Delta\phi_{\omega Tp} = \Delta\phi_{\omega Tp0} + \omega t \tag{A4}$$

Equations (A1–A3) can be rewritten in terms of $\sin\omega t$, $\cos\omega t$ and the four coefficients a_y, b_y, a_z, and b_z:

$$T_n y = a_y\cos\omega t + b_y\sin\omega t \tag{A5}$$

$$T_n z = a_z\cos\omega t + b_z\sin\omega t \tag{A6}$$

where

$$a_y = T_n(\sin\phi_{\omega p}\cos\theta_{\omega p}\cos\Delta\phi_{\omega Tp0} + \cos\phi_{\omega p}\sin\Delta\phi_{\omega Tp0}) \tag{A7}$$

$$b_y = T_n(-\sin\phi_{\omega p}\cos\theta_{\omega p}\sin\Delta\phi_{\omega Tp0} + \cos\phi_{\omega p}\cos\Delta\phi_{\omega Tp0}) \tag{A8}$$

$$a_z = -T_n\sin\theta_{\omega p}\cos\Delta\phi_{\omega Tp0} \tag{A9}$$

$$b_z = T_n\sin\theta_{\omega p}\sin\Delta\phi_{\omega Tp0} \tag{A10}$$

The quantities μ_1, μ_2, μ_3, and μ_4 are defined as

$$\mu_1 = a_y^2 + b_y^2$$

$$\mu_2 = a_z^2 + b_z^2$$

$$\mu_3 = a_y a_z + b_y b_z$$

$$\mu_4 = a_y b_z - b_y a_z \tag{A11}$$

Or in other terms,

$$\mu_1 = T_n^2(\cos^2\theta_{\omega p}\sin^2\phi_{\omega p} + \cos^2\phi_{\omega p}) \tag{A12}$$

$$\mu_2 = T_n^2(\sin^2\theta_{\omega p}) \tag{A13}$$

$$\mu_3 = -T_n^2(\sin\theta_{\omega p}\cos\theta_{\omega p}\sin\phi_{\omega p}) \tag{A14}$$

$$\mu_4 = T_n^2\sin\theta_{\omega p}\cos\phi_{\omega p} \tag{A15}$$

The solution for Eqs. (A12–A15) gives the three unknowns $\theta_{\omega p}$, $\phi_{\omega p}$, and T_n:

$$\sin^2\phi_{\omega p} = 0.5\sqrt{(1-\mu_1/\mu_2)^2 + 4(\mu_3/\mu_2)^2} + 0.5(1-\mu_1/\mu_2) \tag{A16}$$

$$\tan\theta_{\omega p} = -\mu_2/\mu_3\sin\phi_{\omega p} \tag{A17}$$

$$T_n = \sqrt{\mu_2/\sin^2\theta_{\omega p}} \tag{A18}$$

Equations (A9) and (A10) will give $\Delta\phi_{\omega Tp0}$:

$$\Delta\phi_{\omega Tp0} = a\tan^{-1}\left(-\frac{b_z}{a_z}\right) \tag{A19}$$

Acknowledgments

We would like to dedicate this paper to the memory of our coauthor J. V. Breakwell who died on April 16, 1991. We are greatly indebted to him for his keen insights, inspiring leadership, and wonderful sense of humor. He is sorely missed by all those in the Stanford and other academic communities who knew him. We would like to acknowledge the contributions of the many people on the Relativity Gyroscope Program GP-B at Stanford University who contributed to the fabrication, measurement, testing, and operation of the gyroscopes described in this paper. In particular we thank C. W. F. Everitt

and B. Parkinson for their discussion, encouragement, and support; and D. Gill and T. Van Hooydonk for providing the gyroscope coating thickness measurements. Our appreciation goes to M. Jarnot for her keen review of this manuscript.

References

[1]Schiff, L., "Motion of a Gyroscope According to Einstein's Theory of Gravitation," *Proceedings of the National Academy of Science,* April 1960.

[2]Vassar, R., "Error Analysis for the Stanford Relativity Gyroscope Experiment," Ph.D. Thesis, Dept. of Aeronautics and Astronautics, Stanford University, Stanford, CA, 1982.

[3]Everitt, C. W. F., "Report on a Program to Develop a Gyro Test of General Relativity in a Satellite and Associated Control Technology," GP-B TR S0018, W. W. Hansen Lab. of Physics, Stanford Univ., Stanford, CA, June 1980.

[4]Barone, A., and Paterno, G., "Physics and Applications of the Josephson Effect," Wiley, New York, 1982.

[5]Knoebel, H. W., "The Electric Vacuum Gyro," *Control Engineering Journal,* Vol. 11, No. 2, 1964, pp. 70–74.

[6]Phelps, R. K., "Research in Electrostatically Supported Vacuum Gyroscope, Vol. 1, Summary," NASA Rept. N69-19068, NASA Scientific and Technical Information Facility, Washington, DC, Nov. 1968.

[7]Matchett, G. A., "Research in Electrostatically Supported Vacuum Gyroscope, Vol. 2, Electric Torque on an ESVG," NASA Rept. N69-19069, NASA Scientific and Technical Information Facility, Washington, DC, Nov. 1968.

[8]Exworthy, K. W., "Research in Electrostatically Supported Vacuum Gyroscope, Vol. 3, ESVG Suspension Research," NASA Rept. N69-19070, NASA Scientific and Technical Information Facility, Washington, DC, Nov. 1968.

[9]Wacker, J. C., "Research in Electrostatically Supported Vacuum Gyroscope, Vol. 4, ESVG Readout Accuracy Improvement Research," NASA Rept. N69-19071, NASA Scientific and Technical Information Facility, Washington, DC, Nov. 1968.

[10]Matchett, G. A., Phelps, R. K., and Wacker, J. C., "Research in Electrostatically Supported Vacuum Gyroscope, Vol. 5, ESVG Performance," NASA Rept. N72-78992, NASA Scientific and Technical Information Facility, Washington, DC, Nov. 1968.

[11]Eby, P., and Darbro, W., "Electrical Torques on the Electrostatic Gyro in the Gyro Relativity Experiment," NASA TM-78311, NASA Marshall Space Flight Center, AL, Oct. 1980.

[12]Eby, P., "Torques on the Gyro in the Gyro Relativity Experiment," NASA TM-82488, NASA Marshall Space Flight Center, AL, May 1982.

[13]Keiser, G. M., "Suspension Torques on a Gimballed Electrostatically Supported Gyroscope and Requirement on the Gyroscopes and Spacecraft for the Relativity Gyroscope Experiment," GP-B TR S0019, W. W. Hansen Lab., Stanford Univ., Stanford, CA, Feb. 1985.

[14]Keiser, G. M., "Support Dependent Torques in the Relativity Gyroscope Experiment," *Proceedings of the Fourth Marcel Grossman Meeting on General Relativity,* edited by R. Ruffini, North-Holland, Amsterdam, 1986, pp. 465–475.

[15]Parkinson, B. W., Lange, B. O., "The Active Damping of Free-Rotor Gyros," Technical Rept. AFAL-TR-66-229, SUDAAR No. 260, Dept. of Aeronautics and Astronautics, Stanford Univ., Stanford, CA, May 1966.

[16]Everitt, C. W. F., "The Stanford Gyroscope Experiment," *Proceedings of the Conference on Experimental Tests of Gravitation Theories,* Jet Propulsion Lab., JPL TM 33-49, Pasadena, CA, Nov. 1970.

[17]Lockhart, J. M., Cheung, W. S., and Gill, D., "Superconducting Thin-Film Gyroscope Readout for Gravity Probe B," *IEEE Transactions on Instrumentation and Measurement,* Vol. IM-36, No. 2, June 1986, pp. 170–174.

[18]Lockhart, J. M., "SQUID Readout and Ultra-Low Magnetic Fields for Gravity Probe B," *Proceedings of the Society of Photo-Optical Instrumentation Engineers—the International Society for Optical Engineering,* SPIE, Bellingham, WA, Jan. 1986.

[19]Keiser, G. M., and Cabrera, B., "Trapped Flux Readout for an Electrostatically Supported Superconducting Gyroscope," *Proceedings of National Aerospace Meeting of Institute of Navigation,* Inst. of Navigation, Washington, DC, March 1982.

[20]Gill, D., Peters, P., and Sisk, C., "Requirements and an Approach to Coating the Gravity Probe B Gyroscope Rotor," *Proceedings of the 15th International Conference on Metallurgical Coatings* (San Diego, CA), April 1988.

[21]Feteih, S., Keiser, G. M., and Breakwell, J. V., "Mass Unbalance Analysis for GP-B Rotors," *Proceedings of the AIAA Guidance, Navigation, and Control Conference* (Minneapolis, MN), AIAA, Washington, DC, 1988.

[22]Feteih, S., Keiser, G. M., Breakwell, J. V., and Xiao, Y. M., "Results of Dynamic Testing of GP-B Spherical Gyroscopes," *Proceedings of the AIAA Guidance, Navigation, and Control Conference* (Boston, MA), AIAA, Washington, DC, 1989.

[23]Feteih, S., "Dynamically Testing of GP-B Electrostatically Levitated Spherical Gyroscopes," Ph.D. Thesis, Dept. of Aeronautics and Astronautics, Stanford Univ., Stanford, CA, 1989.